GAIT PHASE CLASSIFICATION FOR IN-HOME GAIT ASSESSMENT

Minxiang Ye[1], *Cheng Yang*[1], *Vladimir Stankovic*[1], *Lina Stankovic*[1], *Samuel Cheng*[2]

[1]Department of Electronic and Electrical Engineering, University of Strathclyde, Glasgow, UK
[2]Department of Computer Science and Technology, Tongji University, Shanghai, China

ABSTRACT

With growing ageing population, acquiring joint measurements with sufficient accuracy for reliable gait assessment is essential. Additionally, the quality of gait analysis relies heavily on accurate feature selection and classification. Sensor-driven and one-camera optical motion capture systems are becoming increasingly popular in the scientific literature due to their portability and cost-efficacy. In this paper, we propose 12 gait parameters to characterise gait patterns and a novel gait-phase classifier, resulting in comparable classification performance with a state-of-the-art multi-sensor optical motion system. Furthermore, a novel *multi-channel time series segmentation* method is proposed that maximizes the temporal information of gait parameters improving the final classification success rate after gait event reconstruction. The validation, conducted over 126 experiments on 6 healthy volunteers and 9 stroke patients with hand-labelled ground truth gait phases, demonstrates high gait classification accuracy.

Index Terms— feature extraction, gait phase classification

1. INTRODUCTION

Gait analysis is an essential component in a physical rehabilitation program for stroke survivors and patients with Parkinson's disease who need to relearn normal lower limb motion patterns. Reliable gait analysis, in (near) real time, is challenging due to large amount of data that needs to be processed and the fact that everyone has a unique walking pattern.

Sensor-driven gait analysis has been investigated for decades. Optical, camera-based, motion capture systems use passive (*e.g.*, retro-reflective), active (*e.g.*, LED) or high contrast paper markers with single/multiple high-end RGB/infrared cameras to measure gait [1–6]. EMG/EEG/ECG sensor-based systems acquire muscle status, brain dynamic changes with extra respiration analysis to assess gait functionalities [7–11]. Other systems adopt inertial sensors and force plates [12–15]. Though optical systems have been used as decision support tools in many rehabilitation applications, commercial multi-camera motion analysis systems, such as VICON [1] and Qualisys [2], have drawbacks including large space occupation, complex installation process, poor portability, and high cost.

Alternative, relatively cheaper and portable applications, all based on Microsoft Kinect [16] include: (i) a frailty syndrome detection tool [17] to assess a person's mobility via Timed Up and Go (TUG) tests [18], (ii) tracking the feet motion of patients with neurological impairments for treadmill-based gait training programs [19], (iii) postural control assessment [20] and [21].

The quality of gait assessment not only depends on the accurate motion representation of each joint of interest [22], but also on accurate feature selection and classification from the joint trajectories. Therefore, in this paper, we propose exploiting the trajectories of joints of interest from motion analysis to generate additional features that can be used to better characterise gait, thus improving the quality of gait analysis. The main contributions of this paper are as follows:

1. Autonomous gait pattern extraction methodology
2. A novel, globally optimal feature selection criteria
3. A novel time series classification and gait pattern reconstruction algorithm.

Though we provide experimental results using the Microsoft Kinect v2-based motion capture system of [23], the proposed algorithms can be used with other motion capture systems as they only require as input accurate joint trajectories.

2. RELATED WORK

In [24], a Kinect-based gait assessment system is proposed for normal/abnormal gait classification, where several high-level features are extracted from normal gait analysis and 360° turning analysis to perform statistic features thresholding classification. However, there is no numerical performance report. A point-of-care gait assessment framework that adopts dynamic time warping (DTW), principal component analysis (PCA) and linear discriminant analyses of gait indices is proposed in [25] to quantify gait abnormalities, evaluating limb impairment for patients with multiple sclerosis. However, there is no benchmarking system provided in the study. In [26], motion sequences are segmented into repetitive action sequences based on zero-velocity crossing of the selected representative kinematic parameters that are extracted from a unified representation via a generic full-body kinematic model, unscented Kalman filter, frequency analysis and adaptive k-means clustering. Several filters are introduced in this unsupervised temporal segmentation method which need manual parameter tuning. Experiments are only conducted on easily-distinguishable full-body actions resulting in good performance. However, [26] is not practical for the gait phase segmentation task since it relies on high quality motion representation. A comparable camera-based gait phase classification system is proposed in [3], where the system adopts a single RGB camera to track 2D bull-eye paper markers attached on joints of interest and automatically labels a single frame when one of six gait events of interest occurs via a heuristic thresholding criteria. We have the following improvements: (1) 2D bull-eye paper markers [3] are replaced with retro-reflective ball markers to capture 3D joint location of interests using single depth camera, (2) comprehensive 3D gait parameters based on marker trajectories are defined to cover all possible high-level motion features of each gait phase, and most importantly, (3)

978-1-5090-6067-2/17/$31.00

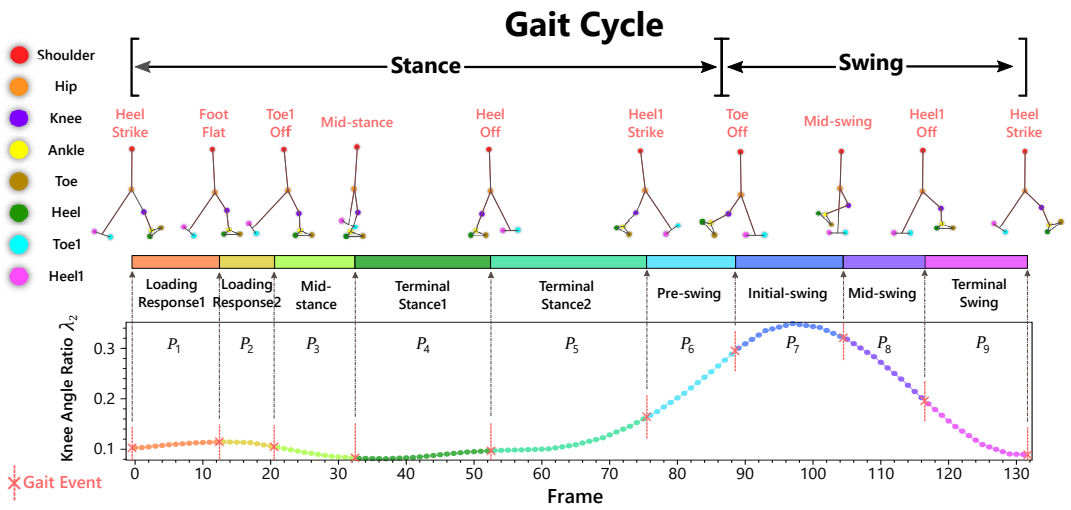

Fig. 1. Definitions of nine gait phases $P_1 - P_9$ (each gait phase is marked by a unique colour). For example, P_1 denotes Loading Response1, and so on. The top of the figure shows nine gait events, with the first event being Heel Strike and so on, using skeleton representation. 8 joints of interest are represented by cycles of different colours. The bottom figure shows a typical curve of knee angle ratio λ_2 during a gait cycle. The remaining gait parameters are defined in Table 1 in order to represent the gait motion.

gait phase classification is done for *all frames* during a gait cycle, unlike [3] that can only detect frames when a gait event occurs.

In [14], gait phase classification, based on a multilayer perception (MLP) neural network (NN) and an NN based on non-linear autoregressive with exogenous inputs (NARX), is used for controlling a lower limb exoskeleton robot ROBIN-H1 by detecting intentions of a small group of healthy volunteers. Pitch orientations and angular velocities of the robot legs are chosen as features of the stance and swing phases for classifier training. The result shows superior system performance with NARX-NN than MLP-NN. However, there is a 5.7% classification success rate (CSR) drop compared to an offline version which achieves 91.93% accuracy. A suitable method for acquiring representative walking pattern data and NN autoencoder is suggested to improve precision.

In [22], artificial neural fuzzy inference systems (ANFIS), autoregressive models with exogenous variables (ARX), output error models (OE), NARX and other NN-based models are compared for gait event detection. Goniometer and foot switches are placed on volunteers leg and footwear to measure the knee flexion/extension angle with foot switches as features. NARX with a 88.59% fit rate is reported as the best model to classify the following gait phases: initial contact, loading response, mid stance, terminal stance, initial swing, mid swing and terminal swing. In this paper, we use the NARX model of [14] as benchmark using 12 gait parameters. Additionally, we propose an autonomous method of feature extraction and classification unlike [14], where these are done manually.

3. GAIT PHASE SEGMENTATION

Gait phase analysis is an assessment method used for gait diagnosis and evaluation popularity [22]. Joint movements of interest are typically used to represent gait motion. Although each individual has a unique walking pattern, each gait phase is discriminable by observing over time the movement pattern of the relevant joints. The extraction of *gait events* comprises gait pattern extraction, gait phase classification and reconstruction that are introduced in the following subsections. In the proposed approach, the segmentation is conducted on $K = 9$ gait phases, labelled as $\{P_1, \ldots, P_K\}$, in order to locate K gait events. Fig. 1 shows the gait events (names are in red on top of the skeletons) based on the trajectories of shoulder, hip, knee, ankle, toe, heel, toe1 & heel1 (opposite side) joints (shown as cycles) captured by a Kinect-based optical motion tracking system [23]. A typical gait phase representation plot is shown at the bottom of the figure based on the ratio of knee angle, where a unique colour is assigned to each gait phase (starting with P_1=Loading Response1 to P_9=Terminal Swing) during the gait cycle. Heel strike event is the first frame of a gait cycle which occurs when the heel marker reaches the floor. To extract a gait cycle from continuous gait motion signals, we adopt *change point detection* on the distance between the heel marker to the floor.

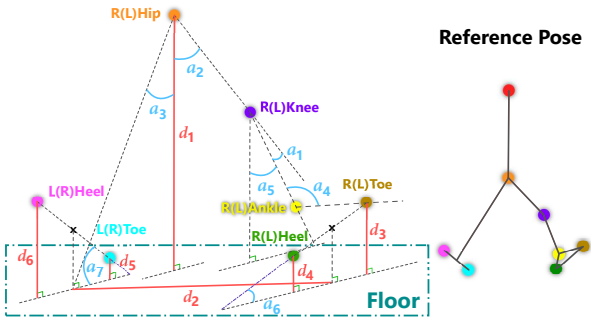

Fig. 2. Visual representation of distances d_i and angles a_i used to define gait intermediate parameters in Table 1. 'x' denotes the centroid of a connection between two joints. All joints are represented by cycles with different colours. R and L stands for Right and Left. For example, L(R)Heel means Left or Right heel joint.

We define *gait parameters*, whose change during the walking exercise will be used to perform gait phase segmentation. Table 1 lists the 12 gait parameters $(\lambda_1, \ldots, \lambda_{12})$, how they are calculated and related physical observations that cover the most important kinematics of each gait phase. A visual representation is shown in Fig. 2.

Table 1. Definitions & observations for selected gait parameters, whose change over time will be used to detect gait events. d_i and a_i are defined in Fig. 2.

Parameter	Value	Observation
foot distance ratio λ_1	$\frac{d_2}{d_1}$	foot switch
knee angle ratio λ_2	$\frac{a_1}{180°}$	limb support
thigh plane angle ratio λ_3	$\frac{a_2}{180°}$	femur swing
toe raise ratio λ_4	$\frac{d_3}{d_1}$	toe contact
heel raise ratio λ_5	$\frac{d_4}{d_1}$	heel contact
toe 1 raise ratio λ_6	$\frac{d_5}{d_1}$	toe 1 contact
heel 1 raise ratio λ_7	$\frac{d_6}{d_1}$	heel 1 contact
leg plane 1 angle ratio λ_8	$\frac{a_3}{180°}$	leg 1 swing
ankle angle ratio λ_9	$\frac{a_4}{180°}$	limb support
shank plane angle ratio λ_{10}	$\frac{a_5}{180°}$	tibia swing
foot angle ratio λ_{11}	$\frac{a_6}{180°}$	foot support
foot 1 angle ratio λ_{12}	$\frac{a_7}{180°}$	foot 1 support

3.1. Gait Pattern Extraction

Based on trajectories of the joints of interest, obtained, for example, by tracking the markers placed on the joints in the recorded video, as in [23], gait parameters are calculated in each frame. For the j-th gait cycle, let $V_j^{\lambda_i}(f)$, $i = 1, \ldots, 12$, denote the value of gait parameter λ_i in the frame f, $f = 1, \ldots, N$.

Gait patterns are characterised by the gait parameters defined previously and are highly subject dependent. Age, associated activity, health, body structure and proportion, all influence gait patterns. To *extract gait patterns* and hence the characteristic gait parameters, we adopt the following three steps: (1) standardising full gait cycles via re-sampling to ensure that each standardised gait cycle is of the same length L; (2) compute a distance matrix for each gait parameter using DTW, supervised using gait phase information; (3) cluster similar gait patterns via density-based spatial clustering of applications with noise (E-DBSCAN) [27] and DTW-Barycenter Averaging (DBA) [28]. We describe these steps next.

Step1: We adopt gait cycle standardisation as an essential step to mitigate walking speed variation across individual gaits. Fig. 3 shows an example how the 12 gait parameters change during normal walk. Since, in general, $V_j^{\lambda_i}$ varies for different j, a new standardised gait parameter function $S_j^{\lambda_i}(x)$, of fixed length of L samples, i.e., $x = 1, \ldots L$, is obtained, by re-sampling $V_j^{\lambda_i}(f)$ via the 2nd-cubic Bezier curve interpolation. For simplicity, we denote S^{λ_i} by S^z, $z \in \{\lambda_1, \ldots, \lambda_{12}\}$.

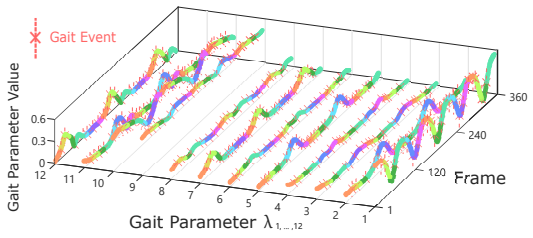

Fig. 3. Typical gait parameter representation plots of normal walk for one gait cycle. Each colour corresponds to a gait phase.

Step2: Cluster analysis of gait patterns is typically used to perform classification tasks such as abnormal gait pattern identification, human recognition, etc. However, only few studies of gait pattern clustering take gait phase information into account. [29] developed a gait phase detection system based on wearable sensors using decision tree to classify level-walking, walking upstairs and walking downstairs based on heuristic rules of gait phase duration. In this paper, we use gait phase transition information to estimate the differences between standardised gait parameters. That is, for $S_i^z(x)$ and $S_j^z(y)$ in the gait cycles i and j, the distance function $\mathbf{\Phi}_{i,j}^z(x, y)$ is defined as:

$$\begin{aligned}\phi(P_a, P_b) = &\frac{K-1}{2} - \Big|\mathbb{1}\big(\lfloor\frac{2|P_a - P_b|}{K+1}\rfloor \bmod 2\big)\cdot \\ &\frac{K-1}{2} - \Big(|P_a - P_b| \bmod \big(\frac{K+1}{2}\big)\Big)\Big|,\end{aligned} \tag{1}$$

$$\mathbf{\Phi}_{i,j}^z(x, y) = \big(S_i^z(x) - S_j^z(y)\big) \cdot \exp\big(\phi(P_{S_i^z}(x), P_{S_j^z}(y))\big). \tag{2}$$

Note that $P_{S_i^z}(x) \in \{1, 2, \ldots, K\}$ is the gait phase label of the gait cycle i and $\mathbb{1}(p)$ is an operator that returns 1 if a Boolean expression p is true, and 0, otherwise. Note that Eq. (2) goes beyond the conventional inner distance function of DTW, as it considers both the numerical difference (the first line of the equation) and the label difference (the exponential factor).

Step3: To cluster similar gait patterns, we adopt E-DBSCAN via DTW with distance function $\mathbf{\Phi}_{i,j}^z(x, y)$ resulting in the individual cluster group $G^z = \{\mathring{S}_1^z, \ldots, \mathring{S}_M^z\}$. After E-DBSCAN clustering, the DBA algorithm is used to extract labelled gait parameters from each cluster group via a distance function $\mathbf{\Psi}_m^z(x, y)$ defined as a distance between the averaged curve $\bar{S}^z$ (a curve that generalizes all curves in the same cluster and is initialized as the curve with min Euclidean distance from all other curves in the same cluster) and any $\mathring{S}_m^z$ in the cluster, given by:

$$\mathbf{\Psi}_m^z(x, y) = \exp\Big(-\bar{\omega}_m^z(x, y) \cdot \big(\mathring{S}_m^z(y) - \bar{S}^z(x)\big)\Big), \tag{3}$$

where shared class weight $\bar{\omega}_m^z(x, y)$ is computed as:

$$\begin{aligned}\bar{\omega}_m^z(x, y) = \frac{1}{KM}\sum_{k=1}^{K}\sum_{m'=1}^{M}\Big(\mathbb{1}\big(P_{\mathring{S}_{m'}^z(y)} = k\big)\Big)\cdot \\ \exp\Big(\phi\big(P_{\bar{S}^z}(x), P_{\mathring{S}_m^z}(y)\big)\Big).\end{aligned} \tag{4}$$

Here, M is the size of the cluster. Note that we count the number of occurrences of the gait phase label P_k in all $\mathring{S}_{1,\ldots,M}^z$ within the same cluster. The distance function in (3) is different from the conventional DTW distance function in that, it is designed to tradeoff the numerical difference between $\mathring{S}_m^z(y)$ and cluster mean $\bar{S}^z(x)$ and the respective difference in gait phase labels $P_{\bar{S}^z}(x) - P_{\mathring{S}_m^z}(y)$.

To obtain the gait phase labels of the average curve, we firstly calculate all wrapped paths between averaged curve and other curves in the same cluster at each iteration of DBA. Secondly, we normalize their costs through min-max standardization. Finally, for each x we count a map of summed path cost for each possible label and then replace the label $P_{\bar{S}^z}(x)$ with the label that results in the minimal summed path cost. The overall motivation is to obtain a good representation of the gait patterns from similar curves but still keeping motion transition information of each gait phase close to the nearest gait event. The resulting series of standardised curves $\bar{S}^z$ are effectively a mean of data reduction from the original $S^z(x)$ curves. For example, during our experiments for each $z \in \{\lambda_1, \ldots, \lambda_{12}\}$, there were 205 samples in S^z which were clustered to between 2 to 7 samples in $\bar{S}^z$. A summary of the gait pattern extraction process is illustrated in Fig. 4.

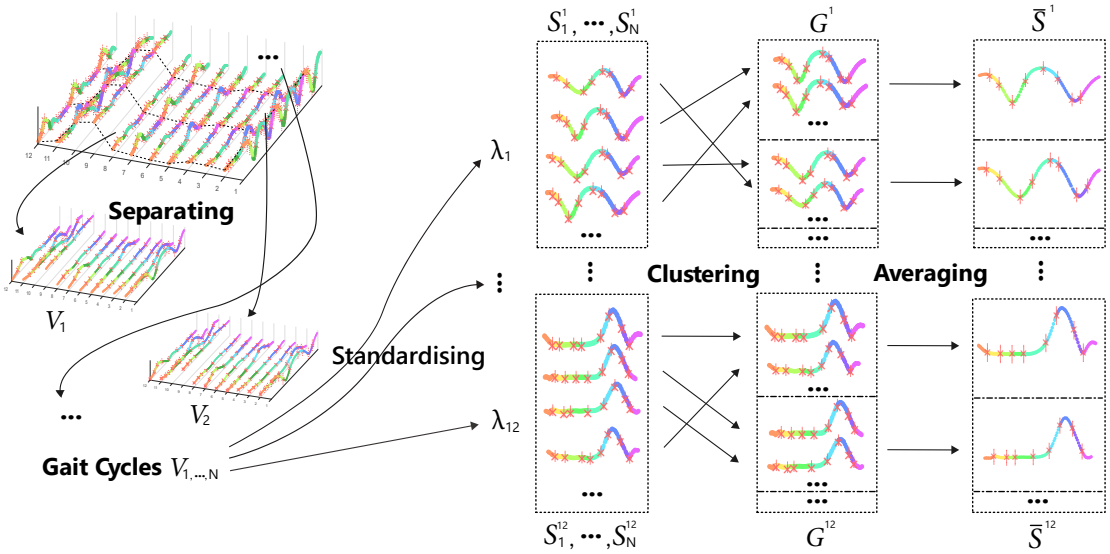

Fig. 4. An illustration of the proposed gait pattern extraction, showing, from left to right, extraction of each of the gait parameters $V^{\lambda_i}(f)$, then standardizing to $S^{\lambda_i}(x)$ (Step1), clustering (Step2) and averaging (Step3).

3.2. Gait Phase Classification

In order to extract linearly separable temporal features, each gait cycle is first segmented based on the heel strike event detection - see Fig. 1. However, since some gait cycles are incomplete, we estimate the length of every incomplete gait cycle from other full gait cycles based on the hip marker speed.

NARX is commonly used for time-series modelling and prediction. Since gait phase classification is a time-series problem that does not require prediction from previous observations, applying the NARX model directly would require an unnecessarily large training time for large-scale datasets. Inspired by image classification studies, such as pose estimation [30], a more robust way to solve this frame-wise time-series classification task is to consider both past and future states. In order to capture the transition information of gait phase labels and gait parameter values near target point $\bar{S}^z(x)$, we make $\bar{S}^z$ periodic such that its starting point is connected to the end point of its replica. Since the standardized interval between each point on curve $\bar{S}^z$ is $1/L$, the standardized time at x is x/L. Then, we define a weak feature candidate pair (u, v) that links any two individual points within a window of length L, centered at x. u and v are chosen as any values within range $[-0.5, 0.5]$ with step of $1/L$ to describe any two points near x.

To capture the time-variant features near x, we define the feature value of a feature candidate pair (u, v) for gait parameter $\bar{S}^z(x')$, $z \in \{\lambda_1, \dots, \lambda_{12}\}$, for all points at standardized times $\{1/L, \dots, 1\}$ inside the L-length window:

$$\Re_l(u, v) = \frac{\|\bar{S}^z(l + uL) - \bar{S}^z(l + vL)\|}{|u - v|}, \tag{5}$$

where we set the length of standardised gait cycle $L = 100$; thus, we have $C_L^2 = 4950$ feature candidate pairs for each gait parameter including $(-0.5, -0.49), (-0.5, -0.48), \dots, (-0.5, 0.5), (-0.49, -0.48), \dots, (0.49, 0.5)$ as (u, v). Since missing feature values often occur near the boundary of the gait parameter curves, we choose enhanced randomized decision forests (ERF) [31] due to the proxy rule for the case of missing features. In order to select those candidate pairs with the most information from the original large-scale data samples V^z, we compute the feature values using (5) from standardised curve $\bar{S}^z$ extracted in Sec. 3.1.

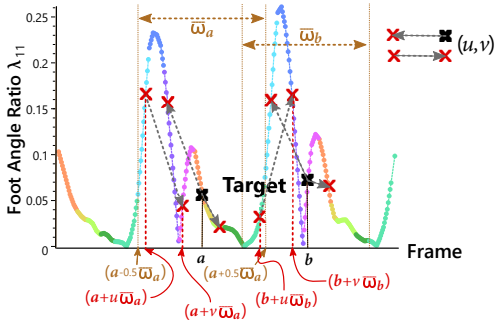

Fig. 5. Feature candidate selection for target frames a and b: different candidate pairs (u, v) result in different responses in terms of foot angle ratio λ_{11}. Similar candidate pairs for all 12 gait parameters can be chosen to classify gait phases.

To ensure that the classifier is not overfitted, we select Ω best feature candidates from a total of C_L^2 candidate pairs, via criteria: (1) Given a finite set of feature candidate pairs $(u, v)_{\varepsilon=1,\dots,C_L^2}$ for each gait parameter, we calculate the quality $Q_\varepsilon^z(P_a, P_b)$ of a feature candidate pair $(u, v)_\varepsilon$ for gait parameter z in terms of gini impurity to split samples with gait phase labels P_a and P_b, $a, b \in \{1, \dots, K\}$. (2) For each gait parameter z, compute total quality Q^z for all possible combinations of gait phase label pairs $Cb_J = \{(P_1, P_2), (P_1, P_3), \dots, (P_2, P_3), \dots, (P_{k-1}, P_k)\}$:

$$Q^z = \sum_{\varepsilon=1}^{C_L^2} \sum_{j=1}^{J} Q_\varepsilon^z(Cb_j). \tag{6}$$

(3) The number of top-ranking pairs with the highest split qualities are selected to maximize the total quality for each gait parameter:

$$num^z = \frac{\Omega \sum_{\varepsilon=1}^{C_L^2} \sum_{j=1}^{J} Q_\varepsilon^z(Cb_j)}{\sum_{z=1}^{12} \sum_{j=1}^{J} Q^z(Cb_j)}. \tag{7}$$

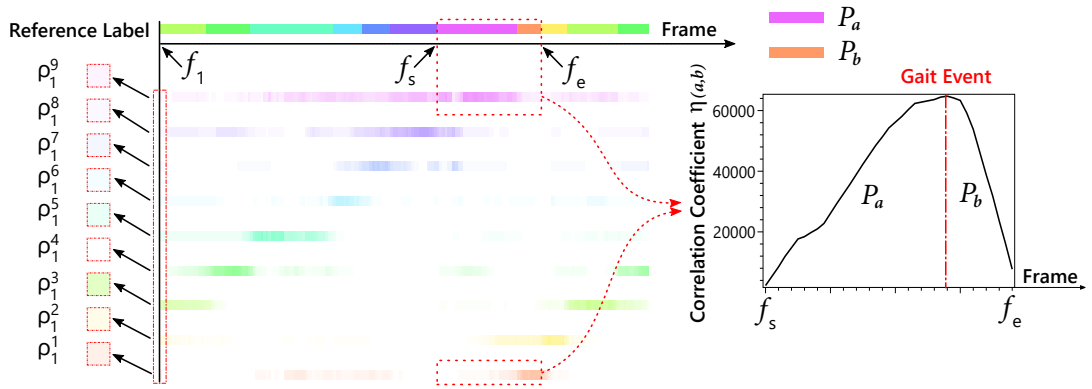

Fig. 6. Class probability and correlation coefficient. The probability value of a class label assigned to a frame is rendered from white to a unique color associated with the class label in ascending order.

During training stage, we use all gait parameter curves V^z in the time domain. In order to capture the same time-variant features near a target frame f via Ω length feature candidate pairs, we map the target point at standardized time t_l into the time domain, where feature candidate pair (u, v) links any two individual frames within a window of length ϖ_f frames, centered at the target frame as illustrated in Fig. 5. The equivalent feature value of a feature candidate pair (u, v) for gait parameter $V^z(f')$ in time domain is calculated by:

$$\Re_f(u,v) = \frac{\|V^z(f+u\varpi_f) - V^z(f+v\varpi_f)\|}{|t^z(f+u\varpi_f) - t^z(f+v\varpi_f)|}. \quad (8)$$

where for a frame f', $t(f')$ denotes the time at which f' is acquired and u and v denotes the normalized offsets from the target frame f, such that $f+u\varpi_f$ and $f+v\varpi_f$ point to the first and the last frame, respectively, in the window centered at frame f.

3.3. Gait Phase Reconstruction

Next, we re-segment each gait phase after ERF-based frame-wise classification using a novel time series reconstruction method. As the gait event occurs between two adjacent gait phases, we can cleverly locate a gait event by detecting the critical state within two adjacent gait phases. Once the gait event is located, the gait phases can be easily segmented.

To locate a gait event, we first obtain a class probability vector $\rho_f = \{\rho_f^1, \ldots, \rho_f^K\}$, given feature values for each frame f from the trained ERF model. The feature vectors are computed across all gait parameters for frame f via Ω feature candidate pairs that are selected, as discussed in in Sec. 3.2.

The class probability vector near gait events is a weak representation of actual gait phases. This weakness is inherited from the weak classification of two nearby classes. Most generic classification algorithms are designed to maximize the differences between classes ignoring the relationships between classes. To address this weakness, we define a correlation coefficient η_f to represent the transition progression of adjacent classes at any frame f. Given continuous frames $f_s, \ldots, f_e$ with two adjacent gait phase labels P_a & P_b, correlation coefficient η_f can be calculated as:

$$\eta_f(a,b) = \sum_{i=f_s}^{f} \rho_i^a \sum_{i=f}^{f_e} \rho_i^b - \sum_{i=f_s}^{f} \rho_i^b \sum_{i=f}^{f_e} \rho_i^a. \quad (9)$$

Given correlation coefficients $\eta_{f_s}(a,b), \ldots, \eta_{f_e}(a,b)$ (see Fig. 6 for an example), we consider the gait event between P_a and P_b located at the frame with global maximum correlation coefficient. Then, we update the gait phases by the detected gait events and iterate until convergence.

4. RESULTS

Experiments are conducted on 9 stroke patients and 6 health volunteers during a 4-meter walking test, resulting in 126 experiments with various walking speed direction and patterns. We acquire estimated trajectories of hip, knee, ankle, toes, heels joints using the motion capture system of [23].

To evaluate the performance of gait phase classification, we divide our dataset into two groups: (1) training set: stroke patients 1-5 and health volunteers 1-3; (2) real-testing set: stroke patients 6-9 and healthy volunteers 4-6. To prove the reliability and validity of the defined 12 gait parameters, we employ the NARX model and NN (Matlab 2016a Neural Time Series toolbox) on the standardized gait cycles during gait pattern extraction. We define individual input sample vector at x as a vector of gait parameter values $S^{\lambda_1}(x), \ldots, S^{\lambda_{12}}(x)$ and train a regression model that outputs its corresponding gait phase label. For the NARX model, input time delays are chosen as 1 to 9 and the Levenberg-Marquardt method is used to train a two-layered NN. In the experiments, 10 networks are generated for each time delay. We randomly choose 70% of training data as training set and 15% of the remaining training data for the train-test set, the remaining 15% are used for validation. Then all 9×10 trained networks are applied on the real-test set. The performance of the NARX model in Table 2 shows stable classification success rates (CSR) for different input delays when using our gait parameters $\lambda_1, \ldots, \lambda_{12}$, defined in Sec.3.

Table 2. Performance (CSR) of the NARX model

Input Time Delays	1	2	3	4	5	6	7	8	9
Train Test	86.5	87.2	87.3	87.9	87.8	88.0	87.8	88.0	87.8
Real Test	82.1	82.6	83.5	82.1	82.2	82.7	82.7	**83.4**	83.4

Using our proposed multi-channel frame-wise time-series classification method, we obtain a significant improvement in CSR compared to the NARX model, as shown in Table 3. Unlike what was done for NARX, we randomly choose 80% of the training data as training set and the rest as train-test set. For each number of features, we obtain the CSR by training 20 sets of decision forests with depth 20 and 30 trees. During the first stage of the gait phase classification, the ERF model is observed to overfit when the feature number

reaches approximately 603 with the highest final CSR after the gait phase reconstruction. We also compare the best CSR for each class between NARX and the proposed method which is shown in Table 4.

Table 3. Performance (CSR) of the proposed method: CSR1 is measured during the first stage of gait phase classification using ERF, CSR2 is the final CSR after gait phase reconstruction.

Feature Count Ω	36	71	149	299	400	603	801	1002
Train Test (CSR1)	82.8	84.9	85.3	87.9	88.1	89.4	91.8	93.8
Real Test (CSR1)	81.2	81.4	82.0	82.9	83.0	**84.1**	84.2	84.2
Real Test (CSR2)	92.5	95.1	96.3	97.8	97.9	**98.4**	98.3	98.2

Table 4. Best performance (CSR) of all K gait phase classes: the input time delay of NARX model is 8; 603 features are used by the proposed method

Gait Phase Class	1	2	3	4	5	6	7	8	9
NARX	82.3	91.2	90.3	90.3	81.9	88.2	92.9	88.5	89.1
Proposed	98.2	99.0	99.2	98.6	97.6	98.7	98.4	98.2	97.8

5. CONCLUSION

This paper proposes a novel approach of extracting and classifying gait patterns to improve the quality of gait phase and gait event classification, enabling improved clinical decision making during gait evaluation. Specifically, gait patterns are extracted via 12 characteristic gait parameters during a 4-meter walking test via supervised clustering that helps feature extraction from the large-scale noisy dataset denoting the calculated values of each gait parameter through data reduction. Globally optimal time series features for all gait parameters are extracted from standardised gait patterns via novel feature selection criteria. These features are then used to generate a comparable gait phase classifier with the state-of-the-art NARX model. In order to segment each phase as piecewise constant signals, we proposed a novel frame-wise multi-channel time-series classification algorithm that obtains significant accuracy improvement as part of a cost-effective, portable gait assessment system.

6. ACKNOWLEDGMENT

This project has received funding from the European Unions Horizon 2020 research and innovation programme under the Marie Skodowska-Curie grant agreement No 734331.

7. REFERENCES

[1] VICON, "Motion capture," http://www.vicon.com, Dec 2016.

[2] Qualisys, "Motion analysis," http://www.qualisys.com, Dec 2016.

[3] C. Yang et al., "Autonomous gait event detection with portable single-camera gait kinematics analysis system," *Journal of Sensors*, Dec 2015.

[4] C. Yang et al., "Human upper limb motion analysis for post-stroke impairment assessment using video analytics," *IEEE Access*, vol. 4, pp. 650 – 659, Feb 2016.

[5] A. Leu et al., "A robust markerless vision-based human gait analysis system," in *IEEE SACI*, May 2011, pp. 415–420.

[6] Y.-R. Li et al., "A gait analysis system using two cameras with orthogonal view," in *Multimedia Technology (ICMT), 2011 Int. Conf.*, July 2011, pp. 2841–2844.

[7] B. J. E. Misgeld et al., "Body-sensor-network-based spasticity detection," *IEEE JBHI*, vol. 20, no. 3, pp. 748–755, May 2016.

[8] C. Zhang et al., "Classification of eeg signals using multiple gait features based on small-world neural network," in *Int. Conf. Ubiquitous Robots and Ambient Intelligence*, Aug 2016, pp. 61–66.

[9] Q. T. Ly et al., "Detection of gait initiation failure in parkinson's disease patients using eeg signals," in *2016 38th Annual Int. Conf. the IEEE EMBC*, Aug 2016, pp. 1599–1602.

[10] Y. D. Xuan et al., "Elderly gait analysis and assessment based on body area network," in *GreenCom IEEE Int. Conf. Cyber, Physical and Social Computing Green Computing and Communications*, Aug 2013, pp. 1729–1733.

[11] M. Derawi et al., "Fusion of gait and ecg for biometric user authentication," in *Int. Conf. BIOSIG*, Sep 2014, pp. 1–4.

[12] "M3d," http://www.tecgihan.co.jp/english/p7.htm, Dec 2016.

[13] Jun-Tian Zhang et al., "Concurrent validation of xsens mvn measurement of lower limb joint angular kinematics," *Physiological Measurement*, vol. 34, no. 8, pp. N63, 2013.

[14] J.-Y. Jung et al., "A neural network-based gait phase classification method using sensors equipped on lower limb exoskeleton robots," *Sensors*, vol. 15, no. 11, pp. 27738–27759, Oct 2015.

[15] J. Taborri et al., "A novel hmm distributed classifier for the detection of gait phases by means of a wearable inertial sensor network," *Sensors*, vol. 14, no. 9, pp. 16212–16234, Sep 2014.

[16] "Developing with kinect for windows," https://dev.windows.com/en-us/kinect/develop, Dec 2016.

[17] E. Gianaria et al., "Kinect-based gait analysis for automatic frailty syndrome assessment," in *IEEE ICIP*, Sep 2016, pp. 1314–1318.

[18] D. Podsiadlo et al., "The timed " up & go": A test of basic functional mobility for frail elderly persons," *Journal of the American Geriatrics Society*, vol. 39, no. 2, pp. 142–148, 1991.

[19] G. Paolini et al., "Validation of a method for real time foot position and orientation tracking with microsoft kinect technology for use in virtual reality and treadmill based gait training programs," *IEEE TNSRE*, vol. 22, no. 5, pp. 997–1002, Sep 2014.

[20] R. A. Clark et al., "Validity of the microsoft kinect for assessment of postural control," *Gait & Posture*, vol. 36, no. 3, pp. 372–377, 3 2012.

[21] Y. Yang et al., "Reliability and validity of kinect rgb-d sensor for assessing standing balance," *IEEE Sensors Journal*, vol. 14, no. 5, pp. 1633–1638, May 2014.

[22] C. Galván-Duque et al., "Comparison between classical and intelligent identification systems for classification of gait events," *J. Control Science and Engineering*, vol. 1, pp. 21–34, 2015.

[23] M. Ye et al., "A depth camera motion analysis framework for telerehabilitation: Motion capture and person-centric kinematics analysis," *IEEE JSTSP*, vol. 10, pp. 877 – 887, Aug. 2016.

[24] J. Zhao et al., "Gait assessment using the kinect rgb-d sensor," in *IEEE EMBC*, Aug 2015, pp. 6679–6683.

[25] F. Gholami et al., "A microsoft kinect-based point-of-care gait assessment framework for multiple sclerosis patients," *IEEE JBHI*, vol. PP, no. 99, pp. 1–1, 2016.

[26] Q. Wang et al., "Unsupervised temporal segmentation of repetitive human actions based on kinematic modeling and frequency analysis," in *3DV 2015*, Nov 2015, pp. 562–570.

[27] P. Sharma et al., *Efficient Density-Based Clustering Using Automatic Parameter Detection*, vol. 1, pp. 433–441, Springer Singapore, 2016.

[28] F. Petitjean et al., "A global averaging method for dynamic time warping, with applications to clustering," *Pattern Recognition*, vol. 44, no. 3, pp. 678 – 693, 2011.

[29] J. S. Wang et al., "Walking pattern classification and walking distance estimation algorithms using gait phase information," *IEE TBME*, vol. 59, no. 10, pp. 2884–2892, Oct 2012.

[30] J. Shotton et al., *Efficient Human Pose Estimation from Single Depth Images*, pp. 175–192, Springer London, 2013.

[31] S. Bharathidason et al., "Improving classification accuracy based on random forest model with uncorrelated high performing trees," *IJCA*, vol. 101, no. 13, pp. 26–30, Sep 2014.